

FLOW STRESS OF STEEL AT LARGE STRAINS AND HIGH STRAIN RATES

G. Pape*, A. Bakker* and M. Janssen*

* Delft University of Technology, Laboratory of Materials Science,
Rotterdamseweg 137, 2628 AL, Delft, The Netherlands

ABSTRACT

In this study an experimental approach has been taken to investigate the strain rate influence on ductile behaviour of steel. A high-rate servo-hydraulic tensile machine has been used to perform experiments on steel. Deformation has been analysed using a high-speed drum-camera. Digital image processing techniques yielded geometry information, which has been used to derive the true stress-strain curve after localisation of deformation. Several correction procedures were applied to derive the von Mises flow stress of the material. Analytical procedures as well as a numerical technique have been used.

A modified Johnson-Cook relation has been applied to fit the experimental data. This relation gives a functional dependence of the material flow stress of the plastic strain and plastic strain rate. The influence of the temperature has been considered as well. The material flow stress increases at increasing strain rate for strains below necking, but tends to decrease at higher strains. The flow stress description used here can only be used for monotonic loading conditions, and does not provide a constitutive model for any deformation history. Modelling of tensile specimen experiments using the strain rate dependent flow stress shows good agreement with measurement data. Localisation behaviour is strongly influenced by the strain hardening and needs a proper description to account for the total deformation.

KEY WORDS

Flow Stress, High Strain Rate, Experiment, Model, Steel, Image Processing

INTRODUCTION

Research for the Royal Netherlands Navy on the vulnerability of warships has resulted in a detailed study on the failure behaviour of explosively loaded panels inside ship structures. This study contains on the one hand a determination of the material response to high strain rate deformation, and on the other hand an investigation of the failure behaviour of the material. Analysis of the failure behaviour was performed experimentally as well as numerically, and also the influence of the strain rate has been taken into account. This paper is concerned with the experimental determination of the flow stress of the material and a proper description of the flow stress as a function of plastic strain and strain rate. Failure investigations have been presented in an additional paper [1].

EXPERIMENTAL TECHNIQUES

The flow-stress of the material can be measured from tensile experiments on smooth round bars. To account for the influence of hydrostatic stress at the neck of the specimen a Bridgman [2], Siebel [3], and Bakker [4] correction procedure have been followed. For the experimental determination of the material flow stress as a function of strain and strain rate, two separate measurement systems have been applied. The first system was applied for strain rates up to 0.1 s^{-1} , the second system for strain rates beyond 10 s^{-1} . Both systems will be shortly discussed here as well as the techniques that have been applied for image processing.

Low Strain Rate Testing

For tensile tests at low strain rates a servo-mechanical machine has been used. Load measurement was provided by a strain gauge loadcell. Extension of the specimen has been measured by a strain gauge extensometer up to the strain at which localisation starts. For strains beyond the onset of necking digital camera images have been used to derive the true strain at the centre of the neck. The true strain ε has been taken from:

$$\varepsilon = \ln \frac{A_0}{A_t} \quad (1)$$

As the rolled plate material shows a slight anisotropy with respect to plastic flow in the plate thickness direction, initially round tensile specimen develop to an oval shape. Therefore two digital cameras were used to measure both diameters of the oval shape, which area has been estimated using an ellipse relation for the cross sectional area at the centre of the neck. Schematically, the camera set-up has been shown in Figure 1.

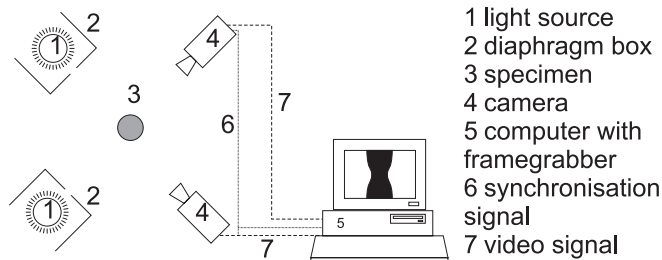


Figure 1: Top view of the camera set-up for the digital imaging system

From the camera images the diameter and radius of curvature of the neck has been derived using image-processing techniques. An anisotropy factor has been derived from the strains from both cameras defined as the quotient of two strain values. This factor appears to be independent of the strain level.

High Strain Rate Testing

The high strain rate testing equipment mainly consists of a hydraulic tensile machine, which can achieve speeds up to 10 m/s. During the experiment a rather constant speed has been maintained. A high-speed camera was used to monitor the deformation in the neck of a specimen. Two markers on the front side of the specimen have been used to measure the elongation during uniform deformation. Images from this conventional rotating drum camera have been developed and scanned with a high-resolution film scanner and subsequently processed with a computer. Image processing techniques will be treated in the next subsection. Load measurement using a piezo-electric loadcell resulted in a vibrating load signal caused by resonance phenomena. Investigations showed that the stresses in the specimen are hardly influenced by these resonances and may be assumed to be equally distributed and without resonance. Smoothing of the

load signal introduced relatively high inaccuracies for the decreasing part of the load curve, the localisation of deformation.

Image Processing

Image processing techniques have been applied to derive geometric data from the recorded images. As the low strain rate experiments have been monitored using digital cameras this resulted in good image quality, facilitating the processing techniques. The digital image was converted into black-white and detection of the specimen contours appeared to be rather simple. A sub-pixel technique was applied to increase the accuracy of the contour positions. Fitting of a circle at a small region of the neck of the specimen yielded an approximation of the radius of curvature, also the diameter has been measured from the images.

At high strain rates the quality of the scanned images was less compared with the digital images and more complicated techniques have been applied for detection of the specimen contours. The main technique consists of taking the second order derivative of the light intensity along a horizontal scan line perpendicular to the specimen axis. The specimen contour is located at a zero value of this derivative. Several smoothing techniques (moving average) were applied to reduce scatter in the derivatives and contour positions.

EXPERIMENTAL RESULTS

Flow Curves at Low Strain Rates

Mateman [5] performed tensile tests at strain rates up to $6.2 \cdot 10^{-2} \text{ s}^{-1}$ (engineering strain rate) using the low rate tensile test equipment. Specimens have been taken in the plate rolling direction, a diameter of 5 mm and gauge length of 35 mm has been chosen. The true failure strain according to Eqn. 1 is smaller for specimen perpendicular to the rolling direction compared to specimen in the rolling direction, respectively 1.0 and 1.46. No remarkable differences have been found in flow stress between the rolling direction and perpendicular to the rolling direction, except for a slightly increased initial yield stress. This means that only the rolling direction has to be examined with respect to flow behaviour. Figure 2 shows a comparison between the flow stress for two material directions taken from experiments.

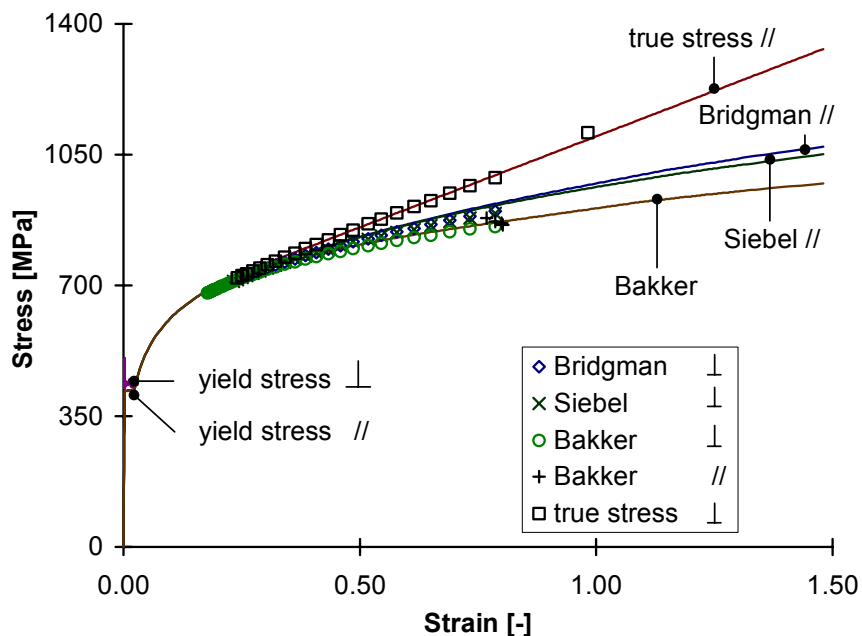


Figure 2. Comparison between flow-stress in parallel (//) and perpendicular (⊥) plate rolling directions

In Figure 2 the one direction is parallel to the rolling direction and shows the average curves for 4 experiments. The second direction is perpendicular to the rolling direction of the plate material and the markers shown in the figure represent only one experiment. To compare these results in both directions, the scatter in measurements for the parallel direction has been presented by plotting a few raw data points of the flow-stress according to Bakker into the graph. These points indicate that no remarkable differences were found between both plate directions. Only the Bridgman flow-stress and Siebel flow-stress deviate a little from the parallel direction. As the axial mean stress and Bakker flow-stress are practically identical and have been derived from load and diameter data only, one can conclude that the ratio a/R is slightly higher in the direction perpendicular to the rolling direction.

Flow Curves at High Strain Rates

For the experiments performed at high strain rate the results showed considerable scatter, as well the strain measurements from the camera images, as the load measurement from the piezoelectric signal. The scatter increased with increasing strain rate as the testing velocity largely influenced resonances. The failure strain appeared to be rather independent of the strain rate, a small reduction of failure strain in the rolling direction was found, yielding a failure strain of 1.3 and 1.4 at engineering strain rates of 60 s^{-1} and 200 s^{-1} , respectively. The correction procedures according to Bridgman [2] and Siebel [3] have been applied. However, the Bakker procedure showed some numerical problems, and an alternative approach has been applied to derive the flow stress at high strain rate. A finite element simulation has been performed using a preliminary flow curve. The flow-curve assumed did not yield to accurate similarity between numerical simulation and experiment. One could observe a premature localisation and deviation of axial stress compared with the experimental data. For this reason, the initial part of the flow-curve up to a strain of 0.2 has been adapted to prevent necking in an early stage of deformation. A simple powerlaw description gave satisfactorily results. For strains larger than 0.2 the coefficients have been adapted to fit the mean axial stress level from the experiment. Table 1 shows the values of the coefficients used in the powerlaw flow-curve. This resulted in a proposed flow curve as has been shown in Figure 3, engineering strain rate is $5.7 \cdot 10^{+1}\text{ s}^{-1}$. Application of this flow-curve resulted in a better agreement between simulation and experiment, although the total elongation still has been underestimated by 10%.

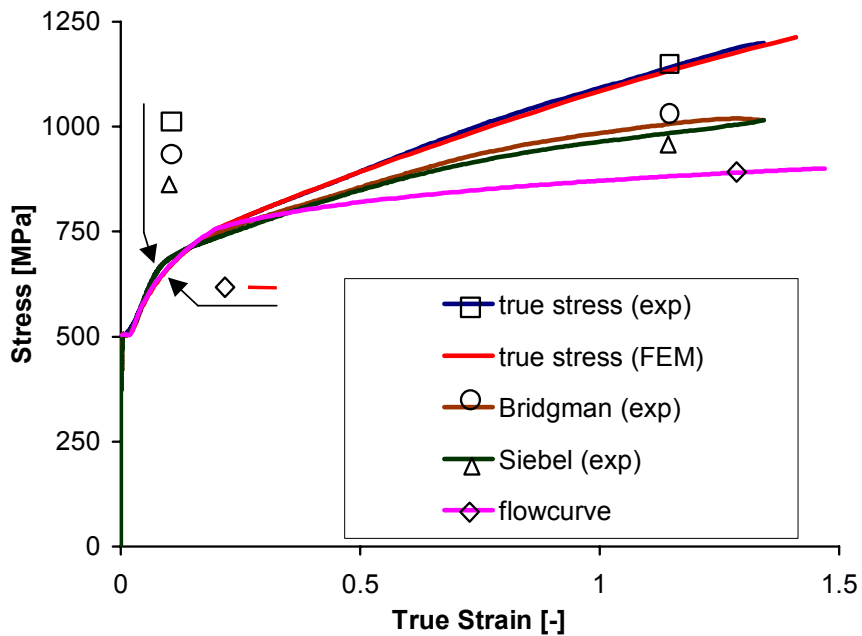


Figure 3: Flow-curve for FEM – simulation that fits experimental curve for the true stress at an engineering strain rate $\dot{\epsilon} = 5.7 \cdot 10^{+1}\text{ s}^{-1}$

TABLE 1.
POWERLAW COEFFICIENTS FOR THE FLOWCURVE AT AN ENGINEERING STRAIN RATE OF $\dot{\epsilon} = 5.7 \cdot 10^{+1} \text{ s}^{-1}$

$\sigma_f = C \varepsilon^n$	C	n
Strain ≤ 0.2	1020 MPa	0.185
Strain > 0.2	871 MPa	0.087

An overview of the flow-stress, which has been derived with the Bakker correction procedure, has been shown in Figure 4. Increasing flow-stress has been observed for strains smaller than 0.4, for large strain values (> 1.4) the flow-stress decreases at increasing strain rate. Note that for strain values in the necking region (larger than 0.2) the strain rate increases at a constant tensile velocity due to necking.

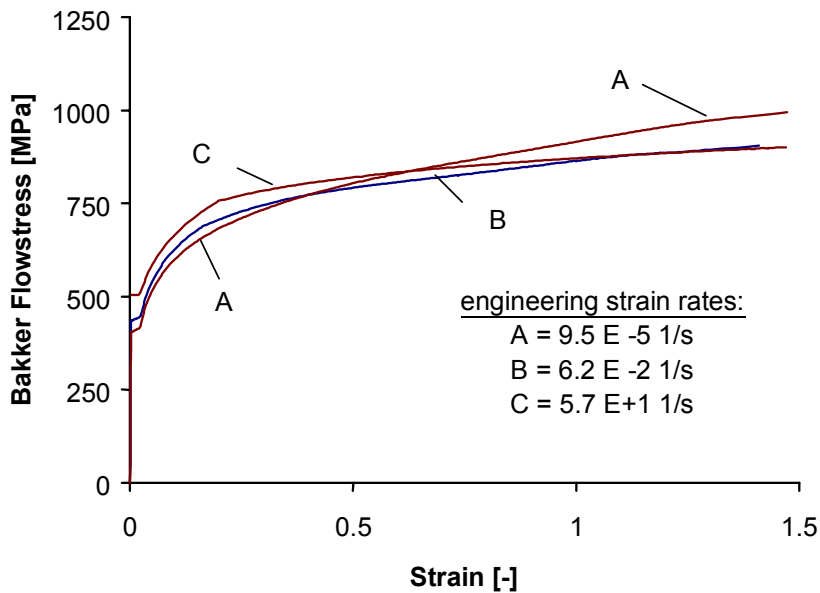


Figure 4: Flow-stress according to Bakker derived from experiments

CURVE FIT OF FLOW STRESS FOR SEVERAL STRAIN RATES

The experimental data has been used to fit a relation between flow-stress, strain, and strain rate. This relation was obtained by modifying the Johnson-Cook [6] relation for varying strain, strain rate, and temperature. We obtained:

$$\sigma_f = [905 + 127 \ln \varepsilon] [1 + C_g (1 - \varepsilon) \ln \dot{\varepsilon}^*] \quad [\text{MPa}] \quad (2)$$

$$\dot{\varepsilon}^* = \frac{\dot{\varepsilon}}{\dot{\varepsilon}_0}; \quad \dot{\varepsilon}_0 = 2.1 \cdot 10^{-3} [\text{s}^{-1}]$$

in which $\dot{\varepsilon}$ denotes the true strain rate, and $\dot{\varepsilon}_0$ is a reference value of the strain rate. For strain values varying from 0 to 0.02 a linear flow-stress has been taken, the level can be obtained by substituting the

strain value of 0.02 in Eqn. 2. Comparing experimental and model flow-stress – strain curves at several strain rates it appears to be a rather good approximation to use the coefficient $C_g = 0.0083$. However, for small strains the increase of flow-stress has been underestimated. A graph has been made for several flow-curves at constant strain rate, shown in Figure 5. Also the strain-hardening exponent derived from the derivative of the power-law function has been plotted into the graph. It has been shown that the necking strain, the intersection point of the hardening exponent and the stability line, decreases slightly with increasing strain rate.

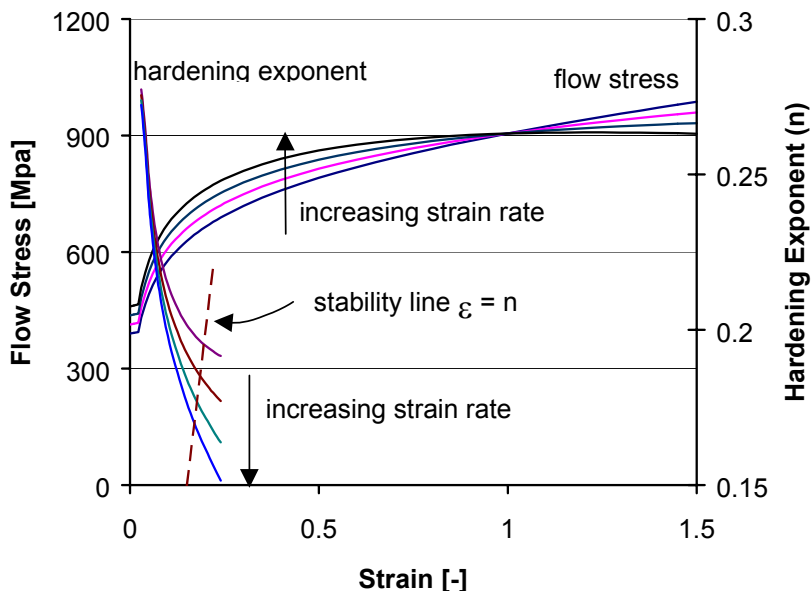


Figure 5: Flow-curves for increasing strain rate, respectively $1 \cdot 10^{-6}$, $1 \cdot 10^{-3}$, $1 \cdot 10^{+0}$, and $1 \cdot 10^{+3} \text{ s}^{-1}$. The hardening exponent has also been given for these strain rates.

ACKNOWLEDGEMENTS

This research was funded by the Technology Foundation STW, the TNO Prins Maurits Laboratory and the Delft University of Technology.

REFERENCES

1. Pape, G., Bakker, A., Janssen, M., (2001) *Fracture Predictions for Ductile Steel*, International Conference on Fracture, ICF 10, Conference Proceedings, Honolulu
2. Bridgman, P.W., (1952) Studies in Large Plastic Flow and Fracture, McGraw-Hill Book Company, New York
3. Siebel, E., (1925) Berichte der Fachausschüsse des Vereins Deutscher Eisenhüttenleute, Werkstoffausschuß, Ber. 71
4. Bakker, A., (1990) *Influence of Material Flow Curve Modelling on Fracture Mechanics Evaluations*, in: Proceedings of the 5th International Conference on Numerical Methods in Fracture Mechanics, Eds. Luxmoore, A.R., Owen, D.R.J.
5. Mateman, G., (1997) *Determination of the Flow-curve of Constructionsteel (in Dutch)*, Graduate Report, Delft University of Technology
6. Johnson G.R. and Cook W.H., (1983) in: Proc. 7th Int. Symposium on Ballistics, The Hague, The Netherlands, 541